# Modeling of Single Noninactivating $Na^+$ Channels: Evidence for Two Open and Several Fast Inactivated States

Yu-Kai The,*† Jacqueline Fernandes,‡ M. Oana Popa,‡ Alexi K. Alekov,‡ Jens Timmer,*† and Holger Lerche‡
*Institut für Physik, and †Freiburger Zentrum für Datenanalyse und Modellbildung, Universität Freiburg, Freiburg, Germany; and
‡Neurologische Klinik und Abteilung für Angewandte Physiologie, Universität Ulm, Ulm, Germany

ABSTRACT Voltage-gated $Na^+$ channels play a fundamental role in the excitability of nerve and muscle cells. Defects in fast $Na^+$ channel inactivation can cause hereditary muscle diseases with hyper- or hypoexcitability of the sarcolemma. To explore the kinetics and gating mechanisms of noninactivating muscle $Na^+$ channels on a molecular level, we analyzed single channel currents from wild-type and five mutant $Na^+$ channels. The mutations were localized in different protein regions which have been previously shown to be important for fast inactivation (D3-D4-linker, D3/S4-S5, D4/S4-S5, D4/S6) and exhibited distinct grades of defective fast inactivation with varying levels of persistent $Na^+$ currents caused by late channel reopenings. Different gating schemes were fitted to the data using hidden Markov models with a correction for time interval omission and compared statistically. For all investigated channels including the wild-type, two open states were necessary to describe our data. Whereas one inactivated state was sufficient to fit the single channel behavior of wild-type channels, modeling the mutants with impaired fast inactivation revealed evidence for several inactivated states. We propose a single gating scheme with two open and three inactivated states to describe the behavior of all five examined mutants. This scheme provides a biological interpretation of the collected data, based on previous investigations in voltage-gated $Na^+$ and $K^+$ channels.

## INTRODUCTION

Voltage-gated $Na^+$ channels are the basis for the initiation and conduction of action potentials in excitable cells. The channel's main $\alpha$-subunit, containing the selectivity filter and the gating machinery of the channel, consists of four domains (D1–D4), each of which contains six transmembrane segments (S1–S6). The S4 segments contain positively charged amino acids constituting the so-called voltage sensors that can move relative to the rest of the protein upon voltage changes. Movement of the voltage sensors out of their resting position upon membrane depolarization leads to an opening of the gate, a process called activation. Conventionally, its reversal upon repolarization, when the channel is transferred back from the open to the closed state, is termed deactivation. During a maintained depolarization, wild-type (WT) $Na^+$ channels, after a brief initial opening, are transferred to another nonconducting state within milliseconds, due to closure of a second gate, and remain closed. This process is called fast inactivation and the conformational state correspondingly, fast inactivated state. A part of the protein located between domains D3 and D4 on the intracellular side of the membrane is responsible for fast inactivation. It is believed that the inactivation gate consists of three-to-four hydrophobic amino acids (isoleucine-phenylalanine-methionine-(threonine), i.e., IFM(T); denoted IFM, thereafter) that might bind to a receptor site within the inner mouth of the pore, blocking the permeation pathway. Previous work revealed the cytoplasmic loops connecting the S4 and S5 segments and the intracellular parts of the S6 segments in D3 and D4 as primary candidates for forming an IFM binding site (1,2).

To deepen the understanding of the molecular mechanism of fast inactivation we performed single channel recordings for channels containing mutations in the regions critical for the fast inactivation process. Analysis of the macroscopic whole-cell currents showed an altered gating of the mutant channels, in particular a disrupted inactivation with a slowing of the current relaxation, the presence of more or less prominent noninactivating, persistent $Na^+$ currents in a range of 3%–55% of the initial peak current and a 10–20 mV positive shift of steady-state inactivation ((3,4), A. Alekov and H. Lerche, unpublished.)

In contrast to macroscopic currents, single ion channel data contain information on the dwell times in different protein conformations and the correlations between them. Thus, they can give further insight into the channel kinetics. Most commonly, single ion channel currents are described by hidden Markov models. In these models, the switching between the different protein configurations, called states, is described by a Markov chain. The number of these states and the allowed transitions between them is comprised graphically in the gating scheme.

One approach to analyze the data has been introduced by Horn and Lange (5). The authors fitted given gating schemes to the idealized, noise-free time series. Since the inevitable antialiasing filter limits the time resolution of the recording system and since the idealization of the current records relies on heavy filtering, brief openings and closings are missed. Several methods to cope with these missed events have been proposed, which are mostly approximative (6–9). An exact solution to the problem of time interval omission has been given by Hawkes

*Submitted August 29, 2005, and accepted for publication December 19, 2005.*
Address reprint requests to Holger Lerche, E-mail: holger.lerche@uni-ulm.de.

0006-3495/06/05/3511/12 $2.00
doi: 10.1529/biophysj.105.073072

et al. (10), who derived recursion formulas for the resulting apparent open and apparent closed time distributions.

In another approach, the noisy time series was directly fitted to a given gating scheme by maximum likelihood methods (11,12). Extensions to cope with colored noise and filtered data have been developed (13–18). All these extensions have the major drawback that they are numerically expensive. We therefore followed the first approach with a correction for missed events and implemented the recursion formulas derived by Hawkes et al. (10) and the approximative solution given by Jalali and Hawkes (19).

In this study, we fitted different gating schemes to the idealized data and compared the models statistically. We intended to deduce kinetic models adequate to describe the data of several mutants and to compare the models of the different channels with respect to their fast inactivation behavior. We observed that for each channel two open states were necessary to comply with the investigated data. Moreover, it is shown that our mutations unmasked three inactivated states which could not be detected for the WT channel. From these considerations, we extracted a single gating scheme for all mutants that was consistent with a biological interpretation.

## METHODS

### Experimental methods

Single $Na^+$ channel data were recorded from human embryonic kidney cells (tsA201) transfected with either WT or one of the mutant $\alpha$-subunits of the adult human skeletal muscle $Na^+$ channel ($Na_V1.4$). We used PCR-based mutagenesis strategies as described in Popa et al. (3). Details of the experimental procedures and primers are available upon request. All mutants were verified by sequencing and assembled in the expression plasmid pRC/CMV.

Whole cell recordings were carried out using an EPC-7 patch-clamp amplifier (List Electronics, Darmstadt, Germany), a Digidata 1200 digitizer and pClamp 6 data acquisition software (Axon Instruments, Union City, CA). The experimental conditions and data analysis were identical with those previously described (3).

For single channel recordings, short electrodes (3 cm) were pulled from borosilicate glass capillaries with an outer diameter of 1.5 mm and an inner diameter of 0.86 mm (Science Products, Hofheim, Germany), covered with Sylgard (Dow Corning, Wiesbaden, Germany), and firepolished to have a final resistance of 4–10 MΩ. They were filled with external recording solution containing NaCl 255, $CaCl_2$ 2.5, KCl 4, TEACl 5, and HEPES 5 (pH 7.3), and backfilled at the end with a little drop of paraffin oil to exclude formation of thin fluid films within pipette and holder (20,21). The recording AgCl wire was immersed through the oil into the pipette solution. The bathing solution contained (in mM): KCl 230, CsCl 20, $MgCl_2$ 1, EGTA 10, and HEPES 5 (pH 7.4). Depolarizing pulses were applied from −120 mV to −20 mV for a duration of 40 ms or 100 ms depending on the activity of the channel. The data were lowpass-filtered at a frequency of 10 kHz with an internal four-pole Bessel filter. For every single channel patch that was taken for evaluation at least 380 up to 1000 sweeps were recorded at a sampling rate of 50 kHz using an Axopatch 200B amplifier and pClamp 8.02 data acquisition. When no overlapping openings were observed, we concluded that there was a single channel in the patch (22).

### Data analysis

Data were filtered digitally with a digital approximation of an eight-pole Bessel filter and a half-amplitude threshold was determined to distinguish closed from open events. Gaussian densities were fitted to the amplitude histograms and the filter frequency was chosen such that random crossings of the threshold were expected to occur rarely. Depending on the data set the filter frequency ranged between 2.5 kHz and 3.5 kHz. A fixed dead time $\tau$ ranging from 90 $\mu$s to 150 $\mu$s was imposed on the data, so that all events shorter than $\tau$ are omitted, and all events longer than $\tau$ are present in the record.

For several kinetic schemes we estimated the rate constants and the initial probability distribution by maximizing the likelihood. To calculate the likelihood we followed the notation of Hawkes et al. (10) and introduced the matrix-valued function ${}^{\mathcal{A}}R(t)$ whose $ij^{\text{th}}$ element describes the probability that the channel is in the open state $j$ at time $t$ and no shut time is detected over the interval $(0, t)$, given that the channel is in the open state $i$ at time zero. We defined the matrix

$$ {}^{\mathrm{e}}G_{\mathcal{AF}}(t) = {}^{\mathcal{A}}R(t-\tau)Q_{\mathcal{AF}}\exp(Q_{\mathcal{FF}}\tau), $$

where $Q$ denotes the generator matrix of the Markov chain, and the sub- and superscripts $\mathcal{A}$ and $\mathcal{F}$ correspond to the open and the closed states, respectively. Similar matrices corresponding to observed closed intervals were introduced by exchanging the symbols $\mathcal{A}$ and $\mathcal{F}$. For one sweep of data consisting of a sequence of observed open and closed time intervals $t_{\mathrm{o1}}, t_{\mathrm{c1}}, \ldots, t_{\mathrm{on}}, t_{\mathrm{cn}}$ the likelihood could be calculated from these matrices as (23–25),

$$ L = \pi_{\mathcal{A}}^{\mathrm{e}}G_{\mathcal{AF}}(t_{\mathrm{o1}})^{\mathrm{e}}G_{\mathcal{FA}}(t_{\mathrm{c1}})\cdots{}^{\mathrm{e}}G_{\mathcal{AF}}(t_{\mathrm{on}})^{\mathcal{F}}R(t_{\mathrm{cn}})u_{\mathcal{F}}. \qquad (1) $$

The $i^{\text{th}}$ entry of the vector $\pi_{\mathcal{A}}$ denotes the probability that the channel is in the open state $i$ at the start of the sweep; $u_{\mathcal{F}}$ is a vector of ones. For the last interval in Eq. 1, the matrix ${}^{\mathcal{F}}R(t)$ instead of ${}^{\mathrm{e}}G_{\mathcal{FA}}(t)$ enters the calculation, which takes account of the fact that the last interval of each sweep is interrupted by the end of the depolarization. For data of several sweeps the values of Eq. 1 for each sweep had to be summed up. The maximization of the likelihood was performed numerically by a quasi-Newton method (subroutine e04ucf of The Numerical Algorithms Group Ltd. (26)).

### Model selection

We started the search with fitting a simple two-state model to the data. We then added one further open or closed state to the resulting model at different positions. From these models we took the one with the largest log-likelihood and added further states successively. When the log-likelihood increased by $>10$ log units, the model with the additional state has been regarded as the better one. The commonly used likelihood ratio test is not applicable here, since the standard conditions are not fulfilled if the two competing models have a different number of states. First, under the null hypothesis one parameter of the larger model lies on the boundary of the parameter space (27). Second and more important, under the null hypothesis a parameter is not identifiable (28,29). The model with an additional state has transition rates that describe the entering and leaving of this state. Under the null hypothesis that the smaller model is true, the rate constant for entering this additional state is zero. The rate constant for leaving this state is undefined and, thus, it is not identifiable. There are no analytical results that take into account the violation of this condition and that can be easily applied to hidden Markov models.

Therefore, when the increase in the log-likelihood was $<10$ log units we applied a parametric bootstrap to decide for or against the more complex model. To this end, we simulated 250 data sets from the smaller model, which has been regarded as the null hypothesis. For each data set, we fitted the models of both the alternative and null hypotheses, and calculated the difference of the log-likelihoods. The empirical distribution of these values gave an approximation to the distribution of the log-likelihood difference under the null hypothesis (30). I.e., we rejected the null hypothesis at the 1% level if the log-likelihood difference found from the data was achieved by $<1\%$ of the simulated data sets. From our experience with simulated data the aforementioned increase of 10 in the log-likelihood leads to very low $p$-values. Moreover, the likelihood ratio test under standard conditions can be used to obtain a rough estimate of the order of magnitude of the $p$-value. The model with an additional state has two further rate constants and one

further parameter for the initial probability distribution. Thus, twice the log-likelihood difference would be $\chi^2$-distributed with three degrees of freedom, resulting in a $p$-value of $p \approx 0.00017$. Taking this as a rule of thumb, the general rejection of the smaller model when the log-likelihood increase is larger than 10 is justified.

Owing to the increasing computational cost, we restricted the model search to models with fewer than eight states. Since the likelihood generally increased only little for models with seven states compared to those with six states, we did not expect that gating schemes with eight states would have improved the fits considerably, with one exception of mutant S4–S5-I1160C/L1482A.

## RESULTS

For our experiments, we chose mutations at three different sites known to be involved in fast inactivation of the voltage-gated $Na^+$ channel:

1. The central phenylalanine of the inactivation particle within the D3–D4-linker (mutation F1311C; see (31)).
2. The S4–S5 loops in domains D3 and D4 (double mutations I1160C/L1482C and I1160C/L1482A; see (3)).
3. The S6 segment in D4 (double mutations F1586C/I1596C and F1586A/I1596A; see (4,32)).

A schematic representation of the channel's $\alpha$-subunit with the indicated mutations is given in Fig. 1 *a*. Macroscopic current recordings for the WT and the mutations are shown in Fig. 1 *b*. The main common alteration in channel gating introduced by all mutations was a distinct level of a persistent, noninactivating $Na^+$ current (F1311C < F1586C/I1596C < I1160C/L1482C < I1160C/L1482A < F1586A/I1596A). We also noticed a slowing of the current decay for the mutants compared to the WT channel; however, this slowing was relatively benign (up to threefold at −20 mV) compared to the huge increase in persistent current (up to 70-fold).

For single channel recordings, we chose a holding potential of −120 mV to ensure that all channels were available for opening. Depolarizing steps were applied to −20 mV, a voltage at which all channels reached their maximal open probability (Fig. 1 *b*, *steady-state activation curves*) and single channel amplitudes still allowed a good resolution of channel openings. For the five mutants, we observed three different gating modes. During the most frequent one, which was observed for >85% of all depolarizing steps, many short openings and closings occurred throughout the whole period of depolarization (Fig. 2 *a*). The second gating mode consisted of traces with a few short openings and long closings (≈15% of depolarizing steps, Fig. 2 *b*). Within the third gating mode, long-lasting bursts of openings (<1% of depolarizing steps, Fig. 2 *c*) were observed. Since the last two gating modes appeared rarely, we could not collect enough data to analyze them with reliable statistics. We therefore

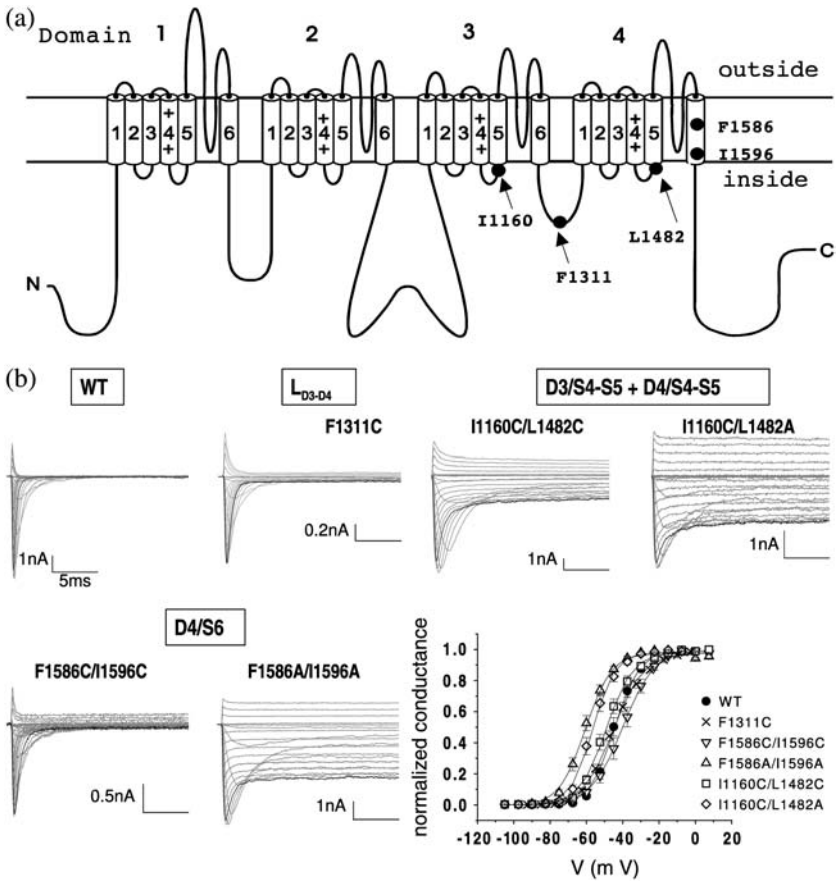


FIGURE 1 Scheme of the $Na^+$ channel $\alpha$-subunit with mutations and macroscopic current recordings. (*a*) Schematic view of the $Na^+$-channel $\alpha$-subunit. The solid line depicts how the amino acid chain of the protein is predicted to be situated in the cell membrane. The vertical cylinders display the six membrane crossing segments (S1–S6) of each domain. Positively charged amino acids conferring voltage dependence to the channel protein (voltage sensors, S4) are symbolized by the + signs. The five sites of the mutations are marked by the circles and/or arrows. (*b*) Whole-cell currents and conductance-voltage relationships of the investigated WT and mutant channels (recorded after depolarizing the membrane from a holding potential of −140 mV in 7.5 mV steps). The trace highlighted in black represents the current elicited by depolarizing the membrane to −22.5 mV. The persistent $Na^+$ current after 70 ms depolarization to −20 mV, evaluated from the whole-cell measurements was as follows: 0.5 ± 0.1% for WT ($n = 9$), 3.6 ± 0.5% for F1311C ($n = 5$), 20.4 ± 1.4% for I1160C/L1482C ($n = 7$), 49.7 ± 3.3% for I1160C/L1482A ($n = 9$), 7.1 ± 0.5% for F1586C/I1596C ($n = 7$), and 55.0 ± 2.8% for F1586A/I1596A ($n = 6$) (means ± SE).

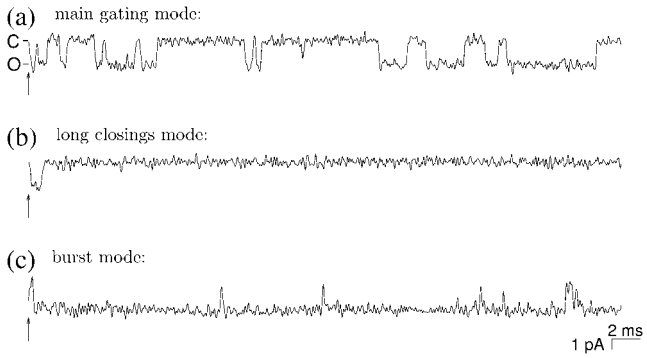


FIGURE 2 Typical current traces representing the three distinct gating modes observed for all mutations shown here for S4-S5-I1160C/L1482A mutant channels. The arrows indicate the onset of the depolarization; *C* marks a closed and *O* an open channel configuration (thus openings are shown as downward deflections). (*a*) The upper trace shows the main gating mode with many short openings and closings. (*b*) The middle trace displays the second mode with a few openings and long closings. (*c*) The last trace shows the third gating mode, which has very long bursts of openings.

restricted the analysis to the main gating mode and selected all such traces visually. For the WT channel, we could not distinguish the main and the second gating modes due to the very few late openings, thus only the third gating mode was excluded from the analysis.

In Table 1 we summarize a selection of the fitted models with their log-likelihood for each channel. For the sake of brevity, we do not show all models that were tried; nevertheless, the presented models will demonstrate how we were led to the best model of each channel. For the final gating schemes we also specify the estimated rate constants and initial probability distributions in Table 2. Indication of error bounds on the parameter estimates has been left to the end of Results, where we present a single common gating scheme that was fitted to all mutants. Since the error bounds of corresponding rate constants are all of the same order of magnitude, the accuracy of the parameters follows from that section.

For all data sets we also fitted models containing loops under the constraint that the principle of microscopic reversibility is obeyed, but none of those improved the log-likelihood for our data. Furthermore, the condition number of the estimated Hessian matrix of the parameters became large indicating that the models with loops were not identifiable for our data (see Discussion).

## The wild-type channel

Table 1 shows a selection of the fitted models with log-likelihoods for the WT channel. The comparison of model 4 with model 2 and of model 10 with model 5 showed that models with two open states fitted the data significantly better than models with a single open state. We performed a parametric bootstrap to test whether or not the log-likelihood difference of nine units between model 16 and model 10 leads to a rejection of model 10. Only one out of the 250 simulated data sets resulted in such a high log-likelihood difference. Thus, we could reject model 10 in favor of model 16 at the 1%-level.

The resulting model 16 with rate constants is shown in Table 2. The estimated probability of being in a particular state at the onset of the depolarization is given by the percentage values in the first row. The steady-state probability distribution indicated in the second row was calculated from the properties of the resulting model 16. The high transition rates directing from $C_1$ toward $C_4$ and the low rates in the opposite direction as well as the high probability of being in $C_1$ at the start of the depolarization suggested that these states correspond to states that were passed through during activation and deactivation. The low rate constant leaving the closed state denoted by *I* justified the identification as the inactivated state. The comparison of models 4 and 12 showed that a second inactivated state did not increase the log-likelihood and, thus, was not supported by our data.

Traces of raw data from the WT channel are displayed in the leftmost diagram of Fig. 3 *a*. The other two diagrams of Fig. 3 *a* show the sum of the currents of all traces and the apparent open time histogram. The solid lines represent the theoretical distributions of the resulting gating scheme 16. The sum current did not fit the theoretical curve exactly but both curves showed qualitatively the same behavior. This deviation suggested that the resulting model 16 was still too simple to reproduce activation properly. The apparent open time histogram agreed well with the theoretical curve.

## Mutant $L_{D3\text{-}D4}$-F1311C

An exact subtraction of capacitive currents due to the voltage pulse was not possible. We therefore had to omit the first three data points (0.06 ms) of every sweep. Some of the fitted models are shown in Table 1. To decide between models 12 and 17 we simulated 500 data sets from model 12 and subtracted the log-likelihood of model 12 from that of model 17 for each data set. The resulting *p*-value was $p \approx 0.007$, i.e., we decided for model 17 at the 1%-level. Since this *p*-value was so close to the 1%-level we decided to simulate 500 data sets instead of 250.

The final gating scheme 17 with rate constants and the initial and steady-state probability distributions are shown in Table 2. Due to the omission of the first three data points of each trace, the initial probability distribution refers to the first analyzed data point instead of the start of the depolarization. From the rate constants and the high probability of being in state $C_1$ at the onset of the voltage pulse, we concluded that the states $C_1$ and $C_2$ were passed through during activation and deactivation. A further closed state for activation/deactivation was not supported (not shown), which was probably related to the omission of the first three data points (see Discussion). The initial and steady-state distributions suggested that $C_3$–$C_5$ correspond to inactivated states. Instead of a

**TABLE 1 Some of the fitted models for each channel with log-likelihood (LL)**

| No. | Model | LL WT | F1311C | S6-C/C | S6-A/A | S4S5-C/C | S4S5-C/A |
|---|---|---|---|---|---|---|---|
| 1 | $C_1 \rightleftarrows O_1 \rightleftarrows C_2$ | −3026 | −41,761 | −33,878 | −136,776 | −34,903 | −86,523 |
| 2 | $C_1 \rightleftarrows C_2 \rightleftarrows O_1 \rightleftarrows C_3$ | −2941 | | | | | |
| 3 | $C_1 \rightleftarrows O_1 \rightleftarrows C_2 \rightleftarrows C_3$ | | −41,669 | −33,848 | −136,641 | −34,662 | −86,413 |
| 4 | $C_1 \rightleftarrows C_2 \rightleftarrows O_1 \rightleftarrows O_2 \rightleftarrows C_3$ | −2928 | | | | | |
| 5 | $C_1 \rightleftarrows C_2 \rightleftarrows C_3 \rightleftarrows O_1 \rightleftarrows C_4$ | −2913 | | | | | |
| 6 | $C_1 \rightleftarrows C_2 \rightleftarrows O_1 \rightleftarrows C_3 \rightleftarrows C_4$ | | −41,608 | | −136,610 | −34,651 | −86,325 |
| 7 | $C_1 \rightleftarrows O_1 \rightleftarrows O_2 \rightleftarrows C_2 \rightleftarrows C_3$ | | | −33,826 | −136,635 | −34,647 | |
| 8 | $C_1 \rightleftarrows O_1 \rightleftarrows C_2 \rightleftarrows O_2 \rightleftarrows C_3$ | | | −33,822 | −136,633 | | |
| 9 | $C_1 \rightleftarrows C_2 \rightleftarrows C_3 \rightleftarrows C_4 \rightleftarrows O_1 \rightleftarrows C_5$ | −2904 | | | | | |
| 10 | $C_1 \rightleftarrows C_2 \rightleftarrows C_3 \rightleftarrows O_1 \rightleftarrows O_2 \rightleftarrows C_4$ | −2899 | | | | | |
| 11 | $C_1 \rightleftarrows C_2 \rightleftarrows O_1 \rightleftarrows C_3 \rightleftarrows O_2 \rightleftarrows C_4$ | | −41,589 | −33,804 | −136,602 | | −86,293 |
| 12 | $C_1 \rightleftarrows C_2 \rightleftarrows O_1 \rightleftarrows O_2 \rightleftarrows C_3 \rightleftarrows C_4$ | −2928 | −41,576 | −33,808 | −136,604 | −34,635 | −86,302 |
| 13 | $C_1 \rightleftarrows C_2 \rightleftarrows O_1 \rightleftarrows C_3 \rightleftarrows C_4$<br>$\updownarrow$<br>$C_5$ | | | | −136,601 | | |
| 14 | $C_1 \rightleftarrows O_1 \rightleftarrows O_2 \rightleftarrows C_3 \rightleftarrows C_4$<br>$\updownarrow$<br>$C_2$ | | | | | −34,631 | |
| 15 | $C_1 \rightleftarrows C_2 \rightleftarrows C_3 \rightleftarrows O_1 \rightleftarrows C_4 \rightleftarrows C_5$ | | | | | | −86,270 |
| 16 | $C_1 \rightleftarrows C_2 \rightleftarrows C_3 \rightleftarrows C_4 \rightleftarrows O_1 \rightleftarrows O_2 \rightleftarrows C_5$ | −2890 | | | | | |
| 17 | $C_1 \rightleftarrows C_2 \rightleftarrows O_1 \rightleftarrows O_2 \rightleftarrows C_3 \rightleftarrows C_4$<br>$\updownarrow$<br>$C_5$ | | −41,572 | | −136,595 | −34,616 | −86,285 |
| 18 | $C_1 \rightleftarrows C_2 \rightleftarrows C_3 \rightleftarrows O_1 \rightleftarrows C_4 \rightleftarrows O_2 \rightleftarrows C_5$ | | | −33,804 | | | −86,238 |
| 19 | $C_1 \rightleftarrows C_2 \rightleftarrows O_1 \rightleftarrows C_3 \rightleftarrows O_2 \rightleftarrows C_4$<br>$\updownarrow$<br>$C_5$ | | | −33,799 | −136,593 | | −86,276 |
| 20 | $C_1 \rightleftarrows C_2 \rightleftarrows C_3 \rightleftarrows O_1 \rightleftarrows O_2 \rightleftarrows C_4 \rightleftarrows C_5$ | | | | | | −86,247 |
| 21 | $C_1 \rightleftarrows C_2 \rightleftarrows C_3 \rightleftarrows O_1 \rightleftarrows C_4 \rightleftarrows O_2 \rightleftarrows C_5$<br>$\updownarrow$<br>$C_6$ | | | | | | −86,217 |

single inactivated state for the WT channel, three distinct inactivated states were necessary to describe the single channel behavior of the mutation.

Fig. 3 *b* shows traces of raw data of the mutant $L_{D3\text{-}D4}$-F1311C. The theoretical predictions of the gating scheme 17 are also compared with the recorded data in Fig. 3 *b*. The sum over all traces and the recorded open times agreed very well with the theoretical curves. The theoretical density (*dotted line*) of the closed times underestimated short and overestimated long dwell times. This was due to the long closed times and the limited duration of the recorded traces, as the last dwell time interval of every trace was interrupted by the end of the voltage pulse. We omitted these time intervals to plot the dwell time histogram. Since the probability of being interrupted by the end of the voltage pulse increased with the duration of an interval, long intervals were disproportionately omitted. Therefore, we also derived the model prediction for the closed time distribution by simulating traces of limited duration. The result is given by the dashed line in the rightmost diagram of Fig. 3 *b*. The agreement with the data was excellent.

## Mutant S6-F1586C/I1596C

A sufficiently exact subtraction of capacitive currents shortly after the onset of the voltage pulse was not possible and we had to omit the first four data points (0.08 ms) of every sweep for the analysis. As shown before for the WT and the other mutant, gating schemes with two open states fitted the data significantly better (Table 1). A parametric bootstrap rejected the null hypothesis that model 11 was preferable to model 19 at the 1%-level. From the 250 simulated data sets the log-likelihood difference of 5 was never achieved.

The resulting gating scheme 19 with rate constants, initial, and steady-state probability distributions is also given in Table 2. Again, the initial distribution refers to the first analyzed data point and not to the start of the voltage pulse. States $C_1$ and $C_2$ were closed states that corresponded to

**TABLE 2 The resulting models for each channel with initial (i.) and steady-state (ss.) probability distribution**

WT Channel: Model 16

$$C_1 \underset{0}{\overset{19234}{\rightleftarrows}} C_2 \underset{0}{\overset{19207}{\rightleftarrows}} C_3 \underset{0}{\overset{10947}{\rightleftarrows}} C_4 \underset{98}{\overset{22403}{\rightleftarrows}} O_1 \underset{858}{\overset{5409}{\rightleftarrows}} O_2 \underset{1.38}{\overset{13319}{\rightleftarrows}} I$$

| | | | | | | | |
|---|---|---|---|---|---|---|---|
| i.: | 75.9% | 0.0% | 0.0% | 0.5% | 0.2% | 0.0% | 23.3% |
| ss.: | 0.0% | 0.0% | 0.0% | 0.0% | 0.02% | 0.0% | 99.97% |

Mutant $L_{D3\text{-}D4}$ F1311C: Model 17

$$C_1 \underset{1}{\overset{9694}{\rightleftarrows}} C_2 \underset{214}{\overset{9936}{\rightleftarrows}} O_1 \underset{1544}{\overset{5527}{\rightleftarrows}} O_2 \underset{75}{\overset{4112}{\rightleftarrows}} C_3 \underset{5}{\overset{3}{\rightleftarrows}} C_4$$

$$254 \uparrow\downarrow 746$$

$$C_5$$

| | | | | | | |
|---|---|---|---|---|---|---|
| i. | 75.3% | 0.0% | 3.5% | 0.0% | 13.8% | 3.2% |
| i. | | | | 4.2% | | |
| ss: | 0.0% | 0.0% | 0.5% | 1.7% | 91.7% | 1.1% |
| ss: | | | | 5.0% | | |

Mutant S6-F1586C/I1596C: Model 19

$$C_1 \underset{1}{\overset{19308}{\rightleftarrows}} C_2 \underset{0}{\overset{9839}{\rightleftarrows}} O_1 \underset{24}{\overset{2976}{\rightleftarrows}} C_3 \underset{5400}{\overset{99}{\rightleftarrows}} O_2 \underset{2}{\overset{38}{\rightleftarrows}} C_4$$

$$279 \uparrow\downarrow 77$$

$$C_5$$

| | | | | | | |
|---|---|---|---|---|---|---|
| i.: | 48.9% | 0.0% | 10.1% | 28.2% | 1.1% | 4.1% |
| i.: | | | | 7.5% | | |
| ss.: | 0.0% | 0.0% | 0.5% | 63.2% | 1.2% | 17.9% |
| ss.: | | | | 17.3% | | |

Mutant S6-F1586C/I1596A: Model 17

$$C_1 \underset{0}{\overset{10295}{\rightleftarrows}} C_2 \underset{378}{\overset{15224}{\rightleftarrows}} O_1 \underset{3275}{\overset{5876}{\rightleftarrows}} O_2 \underset{2513}{\overset{900}{\rightleftarrows}} C_3 \underset{196}{\overset{75}{\rightleftarrows}} C_4$$

$$1286 \uparrow\downarrow 1117$$

$$C_5$$

| | | | | | | |
|---|---|---|---|---|---|---|
| i.: | 54.7% | 0.0% | 0.0% | 21.0% | 0.0% | 0.4% |
| i.: | | | | 24.0% | | |
| ss.: | 0.0% | 0.5% | 19.0% | 34.1% | 12.2% | 4.7% |
| ss.: | | | | 29.6% | | |

Mutant S4-S5-I1160C/L1482C: Model 17

$$C_1 \underset{316}{\overset{42118}{\rightleftarrows}} C_2 \underset{527}{\overset{20078}{\rightleftarrows}} O_1 \underset{626}{\overset{5867}{\rightleftarrows}} O_2 \underset{1972}{\overset{915}{\rightleftarrows}} C_3 \underset{47}{\overset{229}{\rightleftarrows}} C_4$$

$$594 \uparrow\downarrow 2298$$

$$C_5$$

| | | | | | | |
|---|---|---|---|---|---|---|
| i. | 56.0% | 0.0% | 27.5% | 0.0% | 12.3% | 0.3% |
| i. | | | | 3.9% | | |
| ss.: | 0.0% | 0.0% | 1.4% | 13.0% | 6.0% | 29.3% |
| ss.: | | | | 50.2% | | |

Mutant S4-S5-I1160C/L1482A: Model 21

$$C_1 \underset{0}{\overset{16220}{\rightleftarrows}} C_2 \underset{0}{\overset{16203}{\rightleftarrows}} C_3 \underset{13}{\overset{15726}{\rightleftarrows}} O_1 \underset{730}{\overset{643}{\rightleftarrows}} C_4 \underset{12888}{\overset{65}{\rightleftarrows}} O_2 \underset{243}{\overset{7605}{\rightleftarrows}} C_5$$

$$1600 \uparrow\downarrow 506$$

$$C_6$$

| | | | | | | | |
|---|---|---|---|---|---|---|---|
| i.: | 75.0% | 0.0% | 0.0% | 2.4% | 0.0% | 0.2% | 0.0% |
| i.: | | | | | 22.5% | | |
| ss.: | 0.0% | 0.0% | 0.0% | 43.4% | 38.2% | 0.2% | 6.0% |
| ss.: | | | | | 12.1% | | |

activation and deactivation. The comparison of model 18 and model 11 showed that three closed states related to activation were not necessary to fit the data (probably with regard to the omission of the first data points; see Discussion).

Fig. 3 *c* shows traces of raw data of the mutant S6-F1586C/I1596C. Moreover, the theoretical predictions of the model are compared with the data in this figure. All shown properties of the resulting model 19 agreed well with the data. Due to the long closed times, the same problem as with the previous mutant occurred: the omission of the last interval neglected too many long intervals. Therefore, the model prediction was also determined by simulation. It is displayed in the rightmost graph of Fig. 3 *c* as a dashed line.

## Mutant S6-F1586A/I1596A

The log-likelihoods for some of the fitted models of this mutant are shown in Table 1. A parametric bootstrap indicated that model 17 was significantly better than model 13 at the 1% level because the log-likelihood difference of 6 as given in Table 1 has only been achieved by one out of 250 simulated log-likelihood differences. We also performed a parametric bootstrap to test for a significant difference between the nonnested models 17 and 19 by simulating 250 data sets of model 17 and fitting models 17 and 19 to those. The log-likelihood of model 19 was subtracted from the log-likelihood of model 17. The distribution of the log-likelihood differences is displayed in Fig. 4. The dashed line shows the fit of a Gaussian distribution function, which is expected from theory (33). The function can hardly be distinguished from the simulated log-likelihood differences. The arrow marks the value of the log-likelihood difference obtained from the measured data, which yielded a $p$-value of $\sim$0.052; i.e., we could not reject model 17 in favor of model 19 at the 1% level.

The resulting model 17 with rate constants, initial probability, and steady-state probability distribution is given in Table 2. For this mutant two closed states were necessary to describe the activation pathway of the channel satisfactorily. Traces of raw data and the comparison of the distributions predicted by the resulting model with the measured data are given in Fig. 3 *d*. The theoretical curves of the model agreed well with the corresponding histograms of the data.

## Mutant S4-S5-I1160C/L1482C

A smooth subtraction of capacitive currents due to the voltage pulse was not possible and we had to omit the first eight data points (0.16 ms) of every sweep. Table 1 shows the selection of the fitted model with log-likelihoods. Again, all models with two open states fitted the data significantly better than the corresponding models with a single open state.

The resulting model 17 with rate constants and initial and steady-state probability distributions is shown in Table 1. According to the initial distribution, the states $C_1$ and $C_2$

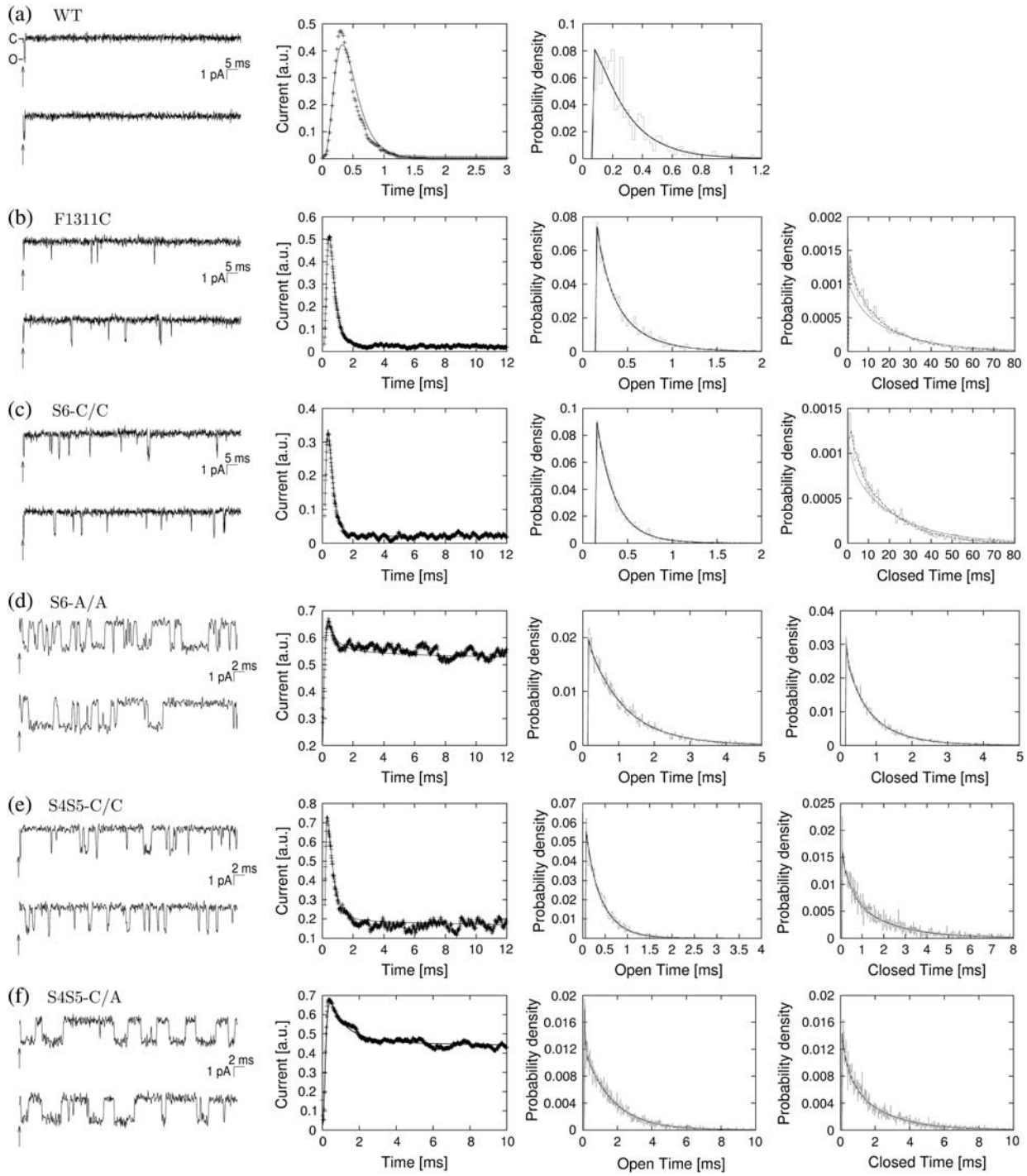


FIGURE 3 Representative traces of raw data from each channel are shown in the leftmost panel of each row. The arrows mark the onset of the depolarization, *C* a closed and *O* an open channel configuration. The other diagrams of each row show the sum over all current traces, the closed time histogram and the open time histogram (from *left* to *right*) for each of the different channels. The solid lines represent the theoretical predictions calculated from the resulting models of each channel given in Table 2. In the rightmost diagram of panels *b* and *c*, the dashed line gives the closed time distribution obtained from simulating the resulting gating scheme. The dotted line gives the theoretical closed time density calculated from the model (for a more detailed explanation, see text).

were related to activation and deactivation, whereas the steady-state distribution suggested that there were three inactivated states ($C_3$–$C_5$). Fig. 3 *e* shows traces of raw data for the mutant S4–S5-I1160C/L1482C. In Fig. 3 *e* we also compared the properties of the resulting gating scheme 17 with the measured data regarding sum current and dwell time distributions. The predicted curves agreed well with our data.

### Mutant S4-S5-I1160C/L1482A

Again, Table 1 summarizes the log-likelihoods for some of the fitted models for this mutant. The comparison of models 12 and 11 with model 6 and of models 20 and 18 with model 15 showed that models with two open states were necessary to comply with our data. The improvement of the log-likelihood of model 19 compared to model 11 suggested to fit the model 21 with eight states to the data of this mutant.

The resulting gating scheme 21 with rate constants and initial and steady-state probability distributions is displayed at the end of Table 2. From the rate constants and the high probability of being in state $C_1$ at the onset of the voltage pulse, we concluded that the states $C_1$–$C_3$ were passed through during activation and deactivation, whereas $C_4$–$C_6$ represented inactivated states. Two traces of raw data are shown in Fig. 3 *f*. The theoretical mean current and apparent open and closed time densities of the resulting gating scheme, shown in the same figure, agreed well with the sum current and the dwell time histograms.

### A comprehensive gating scheme for all mutants

For the six investigated channels we essentially obtained two similar gating schemes. For all mutants at least two closed states were necessary to describe the activation properly. These states were mainly visited at the beginning of the current traces and related to activation and deactivation of the channel. Moreover, for all mutant channels, we found two open states and three further closed states that were mainly visited when the channel had reached an equilibrium after a few milliseconds. Thus, we assumed that these closed states corresponded to distinct inactivated states that were necessary to describe the observed gating behavior with a partial failure of fast inactivation, in contrast to the WT channel for which one inactivated state was sufficient. What encouraged us to fit a common gating scheme to all mutants was the generally good accordance with two open and three inactivated states for all mutants despite their large differences in inactivation failure. In the following the states $C_3$, $C_4$, and $C_5$ will be denoted by $I_1$, $I_2$, and $I_3$, respectively.

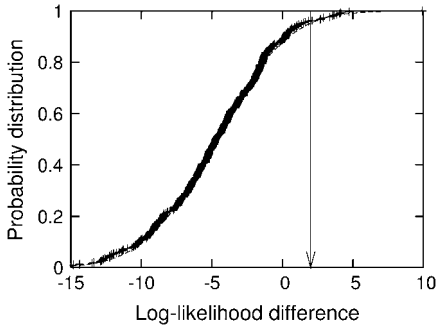


FIGURE 4 Distribution of log-likelihood differences for 250 data sets simulated from the model 17 of mutant S6-F1586A/I1596A. The solid curve shows the fit of a Gaussian distribution function to the data points. The arrow indicates the log-likelihood difference of the measured data. The intersection of the arrow with the Gaussian distribution function yielded a *p*-value of $p \approx 0.052$.

The two resulting gating schemes differed only with respect to the arrangement of the open and inactivated states. For model 17 that was suitable for WT, F1311C, S4-S5-I1160C/L1482C (S4-S5-C/C), and S6-F1586A/I1596A (S6-A/A) the two open states were directly connected. The inactivated states were connected to $O_2$. For model 19 that better fitted S6-F1586C/I1596C (S6-C/C) and S4-S5-I1160C/L1482A (S4-S5-C/A), the two open and two inactivated states alternated. The two submodels that best described the channel's gating behavior in the steady state are sketched in Fig. 5 *a*.

We selected gating scheme 17 with two consecutive open states for further analysis for several reasons. First, two connected open states were found for the WT and the majority of mutant channels. Second, for the two mutants for which model 19 was superior to model 17 the log-likelihood differences between these models were very small compared to the converse differences for the other channels (results not shown). Third, model 17 provided a reasonable biological interpretation for all mutant channels as will be discussed below.

To facilitate a comparison of the different mutants, we used gating scheme 22 in Fig. 5 *b* which, for our data, was equivalent to model 17. Equivalence of models means that they lead to the same observable distributions (34). Note that the gating schemes 17 and 22 are not equivalent in general. For the data presented here, however, the states $C_0$–$C_2$ were almost only visited at the beginning of the current traces, and the remaining states ($O_1$–$O_2$, $I_1$–$I_3$) that were occupied during the steady-state constituted two equivalent gating schemes. The equivalence follows from the existence of a gateway state in both submodels (34,35). Consequently, model 17 and model 22 led to the same log-likelihood (not shown). The state $C_0$ was only included for the S4-S5-C/A mutant. We assume that the main reason for only two closed states supported by the data was the omission of the first few data points due to subtraction artifacts for some of the mutants.

Table 3 shows the estimated rate constants including standard deviations for model 22 for all mutants. For comparison, we added the rate constants from the WT channel for model 16. Concerning activation and deactivation, the transitions from the closed toward the first open state had a high rate, whereas those in the opposite direction had low rates with a high relative error. The rate constants for a transition from $O_1$ to $O_2$ were very similar for all channels, whereas the transition backward rate constants differed by two orders of magnitude, while higher backward rates were associated with a larger persistent $Na^+$ current.

The three inactivated states differed among each other by the frequency they were visited. The rate constants into $I_1$ were high, into $I_2$ intermediate and into $I_3$ low, so that channels

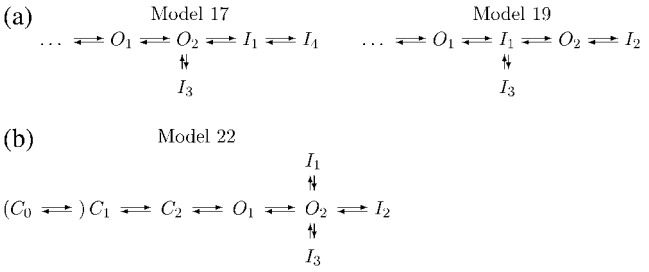


FIGURE 5 (*a*) Submodels of the resulting gating schemes describing the steady-state: The left model fits the WT, F1311C, S4-S5-C/C, and S6-A/A, the right one S4-S5-C/A, S6A/A, and S6-C/C. (*b*) The gating scheme 22 that was fitted to all mutants is shown.

only rarely reached the latter one. With regard to transitions from $O_2$ to the three inactivated states and backward, we also found a generally good correlation between the rate constants and the degree of impaired inactivation, i.e., $O \rightarrow I$ rates were higher for small persistent currents and $I \rightarrow O$ rates were higher for large persistent currents; these correlations were excellent for $O_2 \rightarrow I_1, I_1 \rightarrow O_2, I_2 \rightarrow O_2$, and $I_3 \rightarrow O_2$, while less convincing for $O_2 \rightarrow I_2$ and $O_2 \rightarrow I_3$. Furthermore, large persistent currents were associated with long open and short closed times (Table 3, bottom two lines).

The steady-state probability distributions for all channels are shown in Table 4. The mutants with large persistent currents exhibited a high probability of being in the open states. Among the inactivated states, the probability that a channel occupied state $I_1$ was maximal for all channels, which reflected the high rate of entering that state from $O_2$. Although the rate constant of entering state $I_2$ was generally higher than the corresponding rate for $I_3$, for some mutants the probability of the channel being in $I_2$ was lower than for $I_3$ due to the long dwell time of the latter. The steady-state probabilities for the closed states were essentially zero.

In Table 4 the estimated probabilities of being in a particular state at the time of the first available data point are summarized. The high probabilities for the state $C_0/C_1$ indicated that this was the resting state of the channel. The high initial probabilities of states $I_1$ and $I_2$, respectively, resulted from the lack of direct transitions between the closed and the inactivated states (see Discussion). The omission of the first data points after onset of the depolarization for some of the mutants might also have contributed to this observation.

## DISCUSSION

In this study, we investigated single-channel currents from the WT and five mutants with impaired fast inactivation of the human skeletal muscle $Na^+$-channel. The aim was to find appropriate kinetic models sufficient to describe the distinct gating behavior of the different channels. A detailed microscopic model of $Na^+$ channel gating will be far more complex than the gating schemes presented here, but such a model is likely to be nonidentifiable from single channel currents. Our gating schemes are able to reproduce the behavior of the investigated channels and give insights into the major kinetic states. For the WT channel, similar approaches have been applied by Horn et al. (36), Vandenberg and Bezanilla (37), and Michalek et al. (38). Horn et al. (36) tested among 25 models with one open, one inactivated, and mostly three closed states. The models differed with respect to the parameterization of the rate constants and the allowed transitions between the states. The single-channel analysis by Vandenberg and Bezanilla (37) was performed with nine similar models using different depolarization voltages. Both studies resulted in a gating scheme with three closed states

**TABLE 3 Estimated rate constants for all mutants in $s^{-1}$ for model 22; shown are also the mean values of the closed time (CT) and the open time (OT) in milliseconds**

| | WT | F1311C | S6-C/C | S6-A/A | S4S5-C/C | S4S5-C/A |
|---|---|---|---|---|---|---|
| $C' \rightarrow C_0$ | 19234 ± 7141 | – | – | – | – | – |
| $C_0 \rightarrow C'$ | 0 ± 8 | – | – | – | – | – |
| $C_0 \rightarrow C_1$ | 19207 ± 6921 | – | – | – | – | 16485 ± 3581 |
| $C_1 \rightarrow C_0$ | 0 ± 149 | – | – | – | – | 1 ± 17 |
| $C_1 \rightarrow C_2$ | 10947 ± 1952 | 9711 ± 1808 | 19440 ± 10992 | 10472 ± 3136 | 42204 ± 16140 | 16487 ± 6149 |
| $C_2 \rightarrow C_1$ | 0 ± 3 | 1 ± 26 | 2 ± 77 | 10 ± 142 | 5 ± 241 | 1 ± 17 |
| $C_2 \rightarrow O_1$ | 22403 ± 9769 | 9915 ± 1931 | 9915 ± 3272 | 14734 ± 6182 | 19991 ± 4157 | 15630 ± 2244 |
| $O_1 \rightarrow C_2$ | 98 ± 117 | 215 ± 129 | 50 ± 102 | 311 ± 309 | 534 ± 428 | 25 ± 21 |
| $O_1 \rightarrow O_2$ | 5409 ± 619 | 5517 ± 425 | 4655 ± 472 | 5909 ± 805 | 5897 ± 1067 | 4544 ± 932 |
| $O_2 \rightarrow O_1$ | 858 ± 683 | 1529 ± 407 | 474 ± 150 | 3651 ± 1536 | 649 ± 370 | 11626 ± 4675 |
| $O_2 \rightarrow I_1$ | 13319 ± 3132 | 3927 ± 595 | 4589 ± 364 | 1184 ± 281 | 2306 ± 227 | 2036 ± 932 |
| $I_1 \rightarrow O_2$ | 1 ± 0.4 | 79 ± 8 | 90 ± 5 | 1298 ± 81 | 595 ± 38 | 557 ± 37 |
| $O_2 \rightarrow I_2$ | – | 718 ± 527 | 672 ± 327 | 896 ± 267 | 816 ± 220 | 381 ± 225 |
| $I_2 \rightarrow O_2$ | – | 258 ± 120 | 360 ± 152 | 2651 ± 368 | 2205 ± 559 | 2200 ± 718 |
| $O_2 \rightarrow I_3$ | – | 200 ± 51 | 24 ± 18 | 31 ± 8 | 99 ± 18 | 125 ± 72 |
| $I_3 \rightarrow O_2$ | – | 5 ± 2 | 3 ± 3 | 189 ± 24 | 42 ± 9 | 159 ± 28 |
| CT | – | 16.679 | 17.739 | 1.009 | 1.854 | 1.978 |
| OT | 0.291 | 0.452 | 0.382 | 1.190 | 0.441 | 1.646 |

**TABLE 4 Steady-state and initial probability distribution of all mutants**

| | WT | F1311C | S6-C/C | S6-A/A | S4S5-C/C | S4S5-C/A |
|---|---|---|---|---|---|---|
| | | | Steady-state probability distribution* | | | |
| $C'$ | 0.0% | – | – | – | – | – |
| $C_0$ | 0.0% | – | – | – | – | 0.0% |
| $C_1$ | 0.0% | 0.0% | 0.0% | 0.0 | 0.0% | 0.0% |
| $C_2$ | 0.0% | 0.0% | 0.0% | 0.4% | 0.0% | 0.0% |
| $O_1$ | 0.0% | 0.3% | 0.2% | 20.3% | 1.4% | 33.8% |
| $O_2$ | 0.0% | 1.0% | 1.6% | 32.8% | 12.9% | 13.2% |
| $I_1$ | 99.9% | 51.9% | 81.3% | 29.9% | 50.2% | 48.3% |
| $I_2$ | – | 43.9% | 3.0% | 11.1% | 4.8% | 2.3% |
| $I_3$ | – | 3.0% | 14.1% | 5.4% | 30.6% | 2.3% |
| | | | Initial probability distribution† | | | |
| $t_0$ | 0 $\mu$s | 60 $\mu$s | 80 $\mu$s | 0 $\mu$s | 160 $\mu$s | 0 $\mu$s |
| $C'$ | 75.9% | – | – | – | – | – |
| $C_0$ | 0.0% | – | – | – | – | 70.1% |
| $C_1$ | 0.0% | 75% | 37.4% | 54.7 | 56.0% | 0.0% |
| $C_2$ | 0.6% | 0.0% | 0.0% | 0.0% | 0.0% | 0.0% |
| $O_1$ | 0.2% | 3.5% | 6.7% | 0.0% | 27.5% | 0.0% |
| $O_2$ | 0.0% | 0.0% | 3.2% | 21.1% | 0.0% | 2.6% |
| $I_1$ | 23.3% | 13.0% | 45.3% | 23.8% | 3.8% | 27.3% |
| $I_2$ | – | 4.2% | 3.4% | 0.0% | 11.0% | 0.0% |
| $I_3$ | – | 4.1% | 4.1% | 0.4% | 1.7% | 0.0% |

*The steady-state probabilities were calculated from the estimated parameters of model 22.
†The probabilities at the time $t_0$ of the first available data point were estimated from a fit of model 22. The time point $t_0$ after the onset of the depolarization is given in the second row.

constituting the activation pathway. The third of these states was connected to both the open and the inactivated state. The parameterization was such that two activation and two deactivation rate constants are equal respectively. Transitions leaving the inactivated state were allowed. Michalek et al. (38) obtained a similar gating scheme with only two closed states constituting the activation pathway.

In contrast to these previous studies and to other published models, our final gating scheme for the WT channel contained two contiguously arranged open states. Two open states were also proposed by Armstrong and Bezanilla (39) to explain gating current experiments. Additionally to the voltage sensors they introduced a hypothetical charge that can switch between two positions. The two open states corresponded to both positions of this hypothetical charge. In their model, a typical pathway leading to inactivation appeared exactly as in our model 22. Elinder and Århem (40) have suggested two open states mainly to explain the occurrence of biexponential tail currents.

Chanda and Bezanilla (41) found that the voltage sensor S4 of domain D4 behaves differently from the S4 segments of the other domains using fluorescent labeling of the voltage sensors and combined recordings of voltage sensor movement, gating, and ionic currents. Their experiments showed that the S4 segments in domains D1–D3 moved together with the fast component of the gating current preceding the ionic current, whereas the ionic current preceded movement of D4/S4, which corresponded to the slow phase of the gating current. The authors concluded that the channel opens regardless of the two possible positions of D4/S4. Such a model would match our gating scheme quite nicely, although their model allowed a transition from the first open to an inactivated state. However, the authors emphasized that such pathways were expected to be rarely pursued and we could not find evidence for direct transitions from $O_1$, the state adjacent to the activation pathway, to the inactivated state.

The observation of two open states was consistently confirmed for the mutants. The transition rates from $O_1$ to $O_2$ agreed for all six channels investigated here. Assuming that the mutations did not affect voltage sensor movement, this would be in good agreement with the model of Chanda and Bezanilla (41), relating this transition to the movement of D4/S4. The differences of the rates for the opposite transition ($O_2 \rightarrow O_1$) between mutants with distinct degrees of inactivation failure could be well explained by results of Cha et al. (42), who found that the voltage sensors of domain D3 and D4 were immobilized by inactivation. The mutants S4-S5-C/A and S6- A/A with the highest rates from $O_2$ to $O_1$ had short mean closed times and the largest persistent sodium current, indicating that the inactivation particle was not bound very tightly. Thus, D4/S4 could be less immobilized, and according to Chanda and Bezanilla (41) this would explain the higher backward transition from $O_2$ to $O_1$, reflecting movements of D4/S4. The magnitude of this rate constant was also the main reason for the long open times observed for both mutants.

We obtained very similar gating schemes for all mutations despite their different locations within the channel and their distinct degrees of fast inactivation failure. As already discussed above, model 19, which yielded slightly lower

log-likelihoods for two of the mutants, was rejected mainly for a lack of biological evidence. The similar gating schemes obtained for all mutants provided evidence that these different protein regions are directly or indirectly involved in the same process of fast inactivation. Our results indicated that there are three distinguishable inactivated states for all five mutants, suggesting the inactivation particle could only bind temporarily to more than one receptor site. A plausible explanation for multiple inactivated states would be a sequential binding of the IFM to reach its final site. This could also explain why it was not possible to resolve these states for the WT channel, since they were probably passed rapidly and only in one direction, so that they were not detectable in our single channel recordings. In this regard, we would like to emphasize that, owing to model equivalence, it is not possible to infer the arrangement of the inactivated states from single channel measurements under identical conditions as in this study. For example, as has already been explained previously, models 17 and 22 are equivalent as would be a model with three consecutive inactivated states. A sequential binding of an inactivation particle has been proposed for a voltage-gated inactivating potassium channel by Zhou et al. (43). The authors suggested that the N-terminal inactivation particle first docks to the cytoplasmic surface of the inactivation particle and then binds within the central cavity of the pore. A similar scenario could be well imagined for fast $Na^+$ channel inactivation and would perfectly match our results.

We mainly focused our analysis on open and inactivated states to explain the differences in inactivation of the various mutants. Regarding activation and deactivation, our data do not provide such clear results. For the depolarizing voltage steps used in this study, transitions corresponding to deactivation, i.e., from the open state $O_1$ to the closed states $C_1$–$C_4$, hardly ever occur. Therefore, the rate constants have huge relative errors and are essentially undefined. Moreover, for the WT channel, the resulting model 16 is not able to capture the properties of activation. A more precise analysis of activation and deactivation would require further experiments probably with several different voltage levels.

Direct transitions from the activation pathway to the inactivated states were missing in our models. We tested for them but addition of such loops did not improve the likelihood and the parameters became nonidentifiable. The reason for the nonidentifiability was the rare occupation of the activation pathway in the steady state. Therefore, direct transitions from any closed to an inactivated state would occur mainly at the beginning of the current traces. Since the dwell time of the closed was short compared to the dwell time of the inactivated states, it does not alter the mathematical analysis if the channel is in $C_1$ at the onset of the depolarization and switches directly to the inactivated states or if the channel occupies the inactivated state at the start of the traces.

Nevertheless, these direct transitions are biologically meaningful. The rate constants for such transitions could be estimated when the initial probability of the inactivated states is constrained to zero (44). This would be justified for the WT channel but it could be critical to assume it for the mutants, since the probability that mutant channels were open at the first analyzed data point deviated substantially from zero (see Table 4), which was mainly caused by the omitted data points at the beginning of the recording due to capacitive artifacts. Thus, we could not reliably predict that the channel does not occupy the inactivated states initially.

In summary, the analysis of our single channel data revealed a plausible kinetic gating scheme for voltage-gated sodium channels. We found evidence for two open states, which corresponds well to the observation that the voltage sensor D4/S4 might not be necessary for channel opening (41). Furthermore, the investigation of partially noninactivating mutants unmasked the possible existence of several fast inactivated states, which were not detectable for the WT channel and could probably only be resolved due to the instability of fast inactivation. They might correlate to a sequential binding of the inactivation particle, as it has been proposed for potassium channel N-type inactivation (43).

We thank Dr. Stephanie Schorge for helpful comments on the manuscript.

This work was supported by the Deutsche Forschungsgemeinschaft (DFG grant No. Le1030/5-2 and grant No. Le1030/9-1 to H.L.). H.L. is a Heisenberg fellow of the DFG.

## REFERENCES

1. Catterall, W. A. 2000. From ionic currents to molecular mechanisms: the structure and function of voltage-gated sodium channels. *Neuron.* 26:13–25.
2. Goldin, A. L. 2003. Mechanisms of sodium channel inactivation. *Curr. Opin. Neurobiol.* 13:284–290.
3. Popa, M. O., A. K. Alekov, S. Bail, F. Lehmann-Horn, and H. Lerche. 2004. Cooperative effect of S4–S5 loops in domains D3 and D4 on fast inactivation of the $Na^+$ channel. *J. Physiol.* 561:39–51.
4. Alekov, A., M. O. Popa, E. Derra, F. Lehmann-Horn, and H. Lerche. 2003. A key role of segment D4/S6 in Na channel gating. *Biophys. J.* 84:67a.
5. Horn, R., and K. Lange. 1983. Estimating kinetic constants from single channel data. *Biophys. J.* 43:207–223.
6. Roux, B., and R. Sauve. 1985. A general solution to the time interval omission problem applied to single channel analysis. *Biophys. J.* 48: 149–158.
7. Blatz, A. L., and K. L. Magleby. 1986. Correcting single channel data for missed events. *Biophys. J.* 49:967–980.
8. Magleby, K. L., and D. S. Weiss. 1990. Estimating kinetic parameters for single channels with simulation. *Biophys. J.* 58:1411–1426.
9. Crouzy, S. C., and F. J. Sigworth. 1990. Yet another approach to the dwell-time omission problem of single-channel analysis. *Biophys. J.* 58:731–743.
10. Hawkes, A. G., A. Jalali, and D. Colquhoun. 1990. The distributions of the apparent open times and shut times in a single channel record when brief events cannot be detected. *Philos. Trans. R. Soc. Lond. A.* 332: 511–538.
11. Chung, S.-H., J. B. Moore, L. Xia, L. S. Premkumar, and P. W. Gage. 1990. Characterization of single channel currents using digital signal processing techniques based on hidden Markov models. *Philos. Trans. R. Soc. Lond. B Biol. Sci.* 329:265–285.

12. Fredkin, D. R., and J. A. Rice. 1992. Maximum likelihood estimation and identification directly from single-channel recordings. *Proc. R. Soc. Lond. B Biol. Sci.* 249:125–132.

13. Venkataramanan, L., J. L. Walsh, R. Kuc, and F. Sigworth. 1998. Identification of hidden Markov models for ion channel currents. I. Colored background noise. *IEEE Trans. Signal Process.* 46:1901–1915.

14. Venkataramanan, L., R. Kuc, and F. Sigworth. 1998. Identification of hidden Markov models for ion channel currents. II. State-dependent excess noise. *IEEE Trans. Signal Process.* 46:1916–1929.

15. Venkataramanan, L., R. Kuc, and F. J. Sigworth. 2000. Identification of hidden Markov models for ion channel currents. III. Band-limited, sampled data. *IEEE Trans. Signal Process.* 48:376–385.

16. Qin, F., A. Auerbach, and F. Sachs. 2000. Hidden Markov modeling for single channel kinetics with filtering and correlated noise. *Biophys. J.* 79:1928–1944.

17. Michalek, S., M. Wagner, and J. Timmer. 2000. A new approximate likelihood estimator for ARMA-filtered hidden Markov models. *IEEE Trans. Signal Process.* 48:1537–1547.

18. Fredkin, D. R., and J. A. Rice. 2001. Fast evaluation of the likelihood of an HMM: ion channel currents with filtering and colored noise. *IEEE Trans. Signal Process.* 49:625–633.

19. Jalali, A., and A. G. Hawkes. 1992. Generalised eigenproblems arising in aggregated Markov processes allowing for time interval omission. *Adv. Applied Prob.* 24:302–321.

20. Benndorf, K. 1995. Low-noise recording. *In* Single-Channel Recording. B. Sakmann and E. Neher, editors. Plenum Press, New York. 129–145.

21. Fernandes, J., P. Marvão, A. I. Santos, and P. F. Costa. 2001. Sodium channel currents in maturing acutely isolated rat hippocampal CA1 neurones. *Develop. Brain Res.* 132:159–174.

22. Horn, R. 1991. Estimating the number of channels in patch recordings. *Biophys. J.* 60:433–439.

23. Hawkes, A. G., A. Jalali, and D. Colquhoun. 1992. Asymptotic distributions of apparent open times and shut times in a single channel record allowing for the omission of brief events. *Philos. Trans. R. Soc. Lond. B Biol. Sci.* 337:383–404.

24. Colquhoun, D., A. G. Hawkes, and K. Srodzinski. 1996. Joint distributions of apparent open and shut times of single-ion channels and maximum likelihood fitting of mechanisms. *Philos. Trans. R. Soc. Lond. A.* 354: 2555–2590.

25. Colquhoun, D., C. J. Hatton, and A. G. Hawkes. 2003. The quality of maximum likelihood estimates of ion channel rate constants. *J. Physiol.* 547:699–728.

26. The Numerical Algorithms Group Ltd. 1999. FORTRAN Library Mark 19. The Numerical Algorithms Group, Oxford, UK.

27. Self, S. G., and K. Y. Liang. 1987. Asymptotic properties of maximum likelihood estimators and likelihood ratio tests under nonstandard conditions. *J. Am. Stat. Assoc.* 82:605–610.

28. Davies, R. B. 1977. Hypothesis testing when a nuisance parameter is present only under the alternative. *Biometrika.* 64:247–254.

29. Davies, R. B. 1987. Hypothesis testing when a nuisance parameter is present only under the alternative. *Biometrika.* 74:33–43.

30. Davison, A., and D. Hinkley. 1997. Bootstrap Methods and their Application. Cambridge University Press, Cambridge, UK.

31. Kellenberger, S., T. Scheuer, and W. A. Catterall. 1996. Movement of the $Na^+$ channel inactivation gate during inactivation. *J. Biol. Chem.* 271:30971–30979.

32. McPhee, J. C., D. S. Ragsdale, T. Scheuer, and W. A. Catterall. 1995. A critical role for transmembrane segment IVS6 of the sodium channel subunit in fast inactivation. *J. Biol. Chem.* 270:12025–12034.

33. Vuong, Q. H. 1989. Likelihood ratio tests for model selection and non-nested hypotheses. *Econometrica.* 57:307–333.

34. Kienker, P. 1989. Equivalence of aggregated Markov models of ion-channel gating. *Proc. R. Soc. Lond. B Biol. Sci.* 236:269–309.

35. Fredkin, D. R., M. Montal, and J. A. Rice. 1985. Identification of aggregated Markovian models: application to the nicotinic acetylcholine receptor. *In* Proceedings of the Berkeley Conference in Honor of Jerzy Neyman and Jack Kiefer, Vol. I. L.M. Le Cam and R.A. Olshen, editors. 269–289.

36. Horn, R., C. Vandenberg, and K. Lange. 1984. Statistical analysis of single sodium channels. *Biophys. J.* 45:323–335.

37. Vandenberg, C. A., and F. Bezanilla. 1991. Single-channel, macroscopic, and gating currents from sodium channels in the squid giant axon. *Biophys. J.* 60:1499–1510.

38. Michalek, S., H. Lerche, M. Wagner, N. Mitrovic, M. Schiebe, F. Lehmann-Horn, and J. Timmer. 1999. On identification of $Na^+$-channel gating schemes using moving-average filtered hidden Markov models. *Eur. Biophys. J.* 28:605–609.

39. Armstrong, C. M., and F. Bezanilla. 1977. Inactivation of the sodium channel. II. Gating current experiments. *J. Gen. Physiol.* 70: 567–590.

40. Elinder, F., and P. Århem. 1997. Tail currents in the myelinated axon of *Xenopus laevis* suggest a two-open-state Na channel. *Biophys. J.* 73:179–185.

41. Chanda, B., and F. Bezanilla. 2002. Tracking voltage-dependent conformational changes in skeletal muscle sodium channel during activation. *J. Gen. Physiol.* 120:629–645.

42. Cha, A., P. C. Ruben, J. A. L. George, E. Fujimoto, and F. Bezanilla. 1999. Voltage sensors in domains III and IV but not I and II, are immobilized by $Na^+$ channel fast inactivation. *Neuron.* 22: 73–87.

43. Zhou, M., J. H. Morais-Cabal, S. Mann, and R. MacKinnon. 2001. Potassium channel receptor site for the inactivation gate and quaternary amine inhibitors. *Nature.* 411:657–661.

44. The, Y.-K., J. Fernandes, M. O. Popa, H. Lerche, and J. Timmer. 2005. Estimating rate constants from single ion channel currents when the initial distribution is known. *Eur. Biophys. J.* 34: 306–313.